

# Towards Unbiased Visual Emotion Recognition via Causal Intervention

Yuedong Chen\*

yuedong.chen@monash.edu  
Monash University  
Melbourne, Australia

Tat-Jen Cham

astjcham@ntu.edu.sg  
Nanyang Technological University  
Singapore, Singapore

Xu Yang

101013120@seu.edu.cn  
Southeast University  
Nanjing, China

Jianfei Cai

jianfei.cai@monash.edu  
Monash University  
Melbourne, Australia

## ABSTRACT

Although much progress has been made in visual emotion recognition, researchers have realized that modern deep networks tend to exploit dataset characteristics to learn spurious statistical associations between the input and the target. Such dataset characteristics are usually treated as dataset bias, which damages the robustness and generalization performance of these recognition systems. In this work, we scrutinize this problem from the perspective of causal inference, where such dataset characteristic is termed as a **confounder** which misleads the system to learn the spurious correlation. To alleviate the negative effects brought by the dataset bias, we propose a novel Interventional Emotion Recognition Network (IERN) to achieve the backdoor adjustment, which is one fundamental deconfounding technique in causal inference. Specifically, IERN starts by disentangling the dataset-related context feature from the actual emotion feature, where the former forms the confounder. The emotion feature will then be forced to see each confounder stratum equally before being fed into the classifier. A series of designed tests validate the efficacy of IERN, and experiments on three emotion benchmarks demonstrate that IERN outperforms state-of-the-art approaches for unbiased visual emotion recognition. Code is available at [https://github.com/donydchen/causal\\_emotion](https://github.com/donydchen/causal_emotion).

## CCS CONCEPTS

• **Information systems** → *Multimedia information systems*; • **Human-centered computing** → *Human computer interaction (HCI)*.

## KEYWORDS

Causal intervention, backdoor adjustment, facial expression recognition, image emotion recognition, dataset bias

\*✉ Corresponding Author

Permission to make digital or hard copies of all or part of this work for personal or classroom use is granted without fee provided that copies are not made or distributed for profit or commercial advantage and that copies bear this notice and the full citation on the first page. Copyrights for components of this work owned by others than ACM must be honored. Abstracting with credit is permitted. To copy otherwise, or republish, to post on servers or to redistribute to lists, requires prior specific permission and/or a fee. Request permissions from [permissions@acm.org](mailto:permissions@acm.org).  
MM '22, October 10–14, 2022, Lisboa, Portugal

© 2022 Association for Computing Machinery.  
ACM ISBN 978-1-4503-9203-7/22/10...\$15.00  
<https://doi.org/10.1145/3503161.3547936>

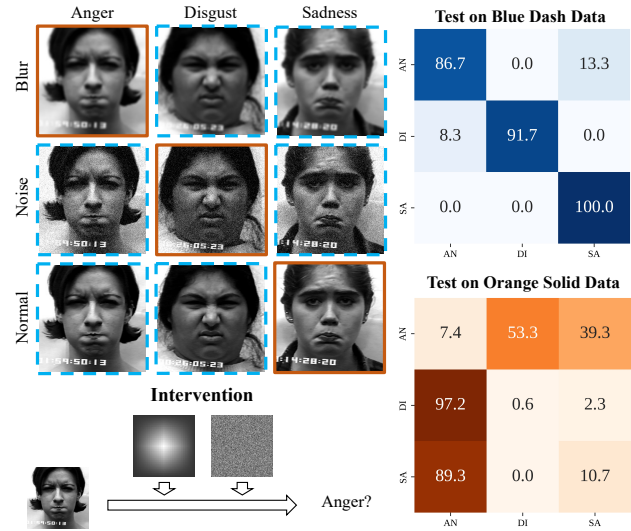


Figure 1: A toy experiment to illustrate the dataset bias problem in facial expression recognition, where different expressions are associated with different types of degradation. A model trained on the blue data performed well when tested on other blue samples (blue confusion matrix), but is impaired dramatically when tested on orange samples (orange confusion matrix). The reason is that the model has been confounded to recognize the more easily learned degradation effects. An intuitive solution is via *intervention* by separately adding blur and noise to all input (bottom left).

## ACM Reference Format:

Yuedong Chen, Xu Yang, Tat-Jen Cham, and Jianfei Cai. 2022. Towards Unbiased Visual Emotion Recognition via Causal Intervention. In *Proceedings of the 30th ACM International Conference on Multimedia (MM '22)*, October 10–14, 2022, Lisboa, Portugal. ACM, New York, NY, USA, 12 pages. <https://doi.org/10.1145/3503161.3547936>

## 1 INTRODUCTION

Visual emotion recognition, including facial expression recognition (FER) [7, 20, 23, 50] and image emotion recognition (IER) [29, 52, 53], has attracted great attention for decades, playing a vital role in lots of daily scenes such as mental health care and driver drowsiness

detection. While deep neural networks (DNNs) show promising performances on several existing benchmarks [10, 21], it has been recently observed that DNNs may “cheat” by relying on unintended cognitive level [58] dataset characteristics, *e.g.*, scene contexts [29] and human attributes [45], instead of the actual affective level [58] causal relationships between the input image and the output emotion label, harming their effectiveness in practice. Intuitively, such dataset characteristics are leveraged by DNNs as the shortcut [14] to learn spurious statistical associations between variables.

DNNs may not appear to be affected by dataset characteristics if the training and test set data are from the same distribution [37], under which most emotion benchmarks are collected and constructed. However, a robust practical emotion recognition system is expected to have consistent generalization even for data from different distributions [37]. Here we design a *toy experiment* to showcase how DNNs behave on data from both the same distribution and different distributions, as depicted in Fig. 1. From a facial expression dataset, we rendered additional images by separately applying blur and noise degradation. They were next partitioned into two datasets (blue dashed vs orange solid borders) by selecting subsets of expressions and degradation labels. A VGG-11 [38] was then trained (randomly initialized and without data augmentation) on samples drawn from the blue dataset. Such a trained model performed well on samples drawn from the same blue dataset (data from the same distribution), shown in the blue confusion matrix of Fig. 1, but is impaired dramatically when tested on samples from the orange dataset (data from a different distribution). Instead of recognizing expressions based on relevant expression features, the model has been biased towards recognizing the degradation effects, which are easier to detect.

Unlike existing methods in emotion recognition that address the dataset bias issue via solutions such as re-sampling and building larger datasets, we choose to leverage **causal inference** [32, 33, 37] to tackle it. In causal inference, entities or attributes that mislead DNNs to learn spurious correlations between input and output are termed as **confounders** [32, 33, 35], which refers to the dataset characteristics in our emotion recognition context. For example, in the above toy experiment, the model has been misled to confound *blur* with *disgust* and *sadness*, and fails to recognize *anger* when *blur* co-occurs. An intuitive solution for the toy experiment is to add noise or blur to all input images (see the bottom left of Fig. 1), whose underlying principle is to deconfound the emotion recognition systems from the confounder / dataset characteristics. This solution is also known as **causal intervention** [32].

To deal with more sophisticated confounders, *i.e.*, *unknown dataset characteristics* and *image scenes*, we analyze the problem with Pearl’s structure causal model (SCM) [32], and propose a novel framework we call **Interventional Emotion Recognition Network (IERN)**, to do the intervention by embedding the **backdoor adjustment** theorem [32]. Although backdoor adjustment has been incorporated in some recent deep learning models for other vision tasks [12, 40, 51], all of these only *approximate* the intervention via memory-query operations, rather than applying *real* intervention as is done in our IERN.

Specifically, our IERN starts by disentangling the dataset-related context feature from the actual emotion feature, where the former represents the confounder. Following application of the backdoor

adjustment theorem, the emotion feature will then be forced to see each confounder stratum equally before being fed into the classifier. We showcase how IERN realizes the backdoor adjustment theorem effectively on the facial expression recognition task via a mixed-dataset configuration, where emotion-independent dataset characteristics are treated as confounder, with dataset name being the label. On the image emotion recognition task, IERN outperforms the state-of-the-art approach by a significant margin under the challenging cross-dataset setting, where image scenes are treated as confounders. The contributions are threefold,

- We are the first to tackle dataset bias in visual emotion recognition from a causality perspective.
- We propose a novel trainable framework, named Interventional Emotion Recognition Network (IERN), to realize the backdoor adjustment theorem.
- With rigorous experiments done for both the mixed-dataset and cross-dataset on existing benchmarks, we show how IERN effectively alleviates negative effects raised by dataset bias and outperforms state-of-the-art approaches.

## 2 RELATED WORK

*Visual Emotion Recognition.* The majority of emotion recognition works belong to **Facial Expression Recognition (FER)**, where the input are human facial images with simple and limited backgrounds [16, 43, 57]. Most methods focus on enhancing performance by making use of related auxiliary priors, *e.g.*, facial landmarks [19, 55, 56], local regions [9, 17, 48], action units [7, 8, 24], optical flows [39], *etc.* The assumption of these methods is that the training data is fairly distributed, which may be wrong and could harm the generalization performance of trained models. Recently, the bias problem has received much attention, and most approaches [13, 22, 28, 36] mainly aim to intuitively disentangle the bias features, so as to build more robust emotion features.

Others belong to **Image Emotion Recognition (IER)**, which aims to recognize the emotions invoked from images that contain a variety of objects rather than recognizing emotions of human faces. Approaches along this line mainly deal with social media photos [44, 47], manually generated images [18], artistic photographs [1, 58], web crawled natural images [29, 52, 53], *etc.* The most relevant work is [29], which identified the image scene as the bias factor, and managed to alleviate the bias issue by building a new larger and more balanced dataset using web data.

Different from all approaches that handle dataset bias in visual emotion recognition via heuristic solutions, our approach is the first to offer a fundamental understanding of the bias issue via causal inference, and propose a new trainable unbiased framework based on causal intervention, by employing the feature disentanglement technique and the center loss function [46].

*Causal inference.* Causality [32, 35, 37] can help pursue the causal effect between two observed variables, rather than depend only on their correlation. Many works have been proposed to explore how causality can be leveraged in machine learning [4, 5, 27, 30]. Recently, causal inference has been introduced into the deep learning framework for several computer vision tasks, including image captioning [51], image classification [6, 25, 40], semantic segmentation [12], and few-shot learning [54].

Our work differs from causality-based deep learning methods in two aspects. Firstly, ours is the first to address the biased visual emotion recognition problem. Secondly and more importantly, we propose a novel solution by learning confounder features and conducting *real* intervention, while previous methods had chosen to model confounders using a predefined dictionary and approximate intervention via memory-query operations by adopting the Normalized Weighted Geometric Mean (NWGM) [3, 49].

### 3 METHODOLOGY

Given input image  $X$ , visual emotion recognition aims to solve the problem  $P(Y|X)$ , where  $Y$  is the emotion label. In this section, we will detail how confounder  $D$  undermines the objective of  $P(Y|X)$  (Section 3.1) to raise dataset bias, how such a bias effect can be removed (Section 3.2), and what our unbiased solution is (Section 3.3).

#### 3.1 SCM for Emotion Recognition

Structural causal models (SCM) [32, 37] are designed to analyze the causal relationships. Fig. 2 shows a SCM in our context constructed among input  $X$ , emotion  $Y$  and confounder  $D$ . The direction of an edge denotes only the causal relationship, while information can flow bidirectionally, e.g.,  $D \rightarrow X$  means that  $D$  is the cause and  $X$  is the effect, while information can still flow from  $X$  to  $D$ .

$X \rightarrow Y$ . It is the intended causal relationship that the network is supposed to learn, which is to recognize emotion  $Y$  based on input image  $X$ . For simplicity, we mix the use of symbol  $X$ , denoting either input images or image features.

$D \rightarrow X, D \rightarrow Y$ . Confounder  $D$  is the undesirable context feature, e.g., *unknown dataset characteristics, image scenes*. Without disentanglement, confounder are normally embedded in the input features, and thus we have  $D \rightarrow X$ . Similarly, confounder also affects networks in predicting emotion, so we have  $D \rightarrow Y$ .

$X \leftarrow D \rightarrow Y$  (*backdoor path*). The existence of confounder  $D$  enables a backdoor path between  $X$  and  $Y$ , by which networks can be biased to build up spurious correlation between  $X$  and  $Y$ , leading to degradation of its generalization performance. For example, as shown in Fig. 1, instead of identifying the correct *anger* image features to recognize *anger*, i.e.  $X \rightarrow Y$ , networks may learn that *noise* is *anger*, i.e.  $D \rightarrow X$ , and should be predicted as *anger*, i.e.  $X \leftarrow D \rightarrow Y$ .

The backdoor path can be explained with the law of total probability. Specifically,  $P(Y|X)$  can be decomposed into

$$P(Y|X) = \sum_d P(Y|X, D = d)P(D = d|X), \quad (1)$$

where  $d$  is one of the strata (a.k.a. “level”) of confounder  $D$ , e.g.,  $d_{\text{blur}}$ ,  $d_{\text{noise}}$ . Assuming that spurious correlation leads to  $P(d_{\text{noise}}|X_{\text{anger}}) \approx 1$ , then  $P(Y|X_{\text{anger}})$  will become  $P(Y|X_{\text{anger}}, d_{\text{noise}})$ , resulting in bias towards  $d_{\text{noise}}$ .

#### 3.2 Intervention with Backdoor Adjustment

Once the confounder is identified, a straightforward solution to alleviate the dataset bias is to build a larger dataset to ensure that emotion is balanced among all confounder strata, similar to what

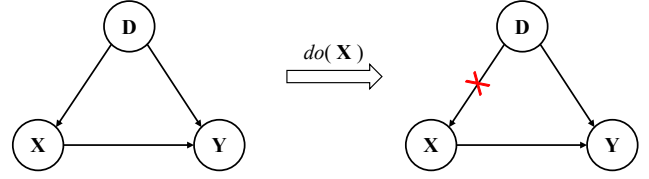


**Figure 2: Left: structural causal model (SCM) for visual emotion recognition. Right: intervention with backdoor adjustment. The direction of an edge denotes only the causal relationship, pointing from the cause to the effect, while information can flow bidirectionally.  $X, Y, D$  refer to input image, emotion label and confounder, respectively.**

has been done in [29]. However, such solutions might not be practical due to three main reasons. Firstly, it is time-consuming and costly to collect and label a large amount of data. Secondly, if the confounder is too complex, it is hard to construct a balanced new dataset. Thirdly, there may be ethical or practical issues in collecting certain types of data, e.g., forcing a child to cry in a park in order to get negative-emotional park images.

We therefore turn to a more elegant solution of applying the **intervention** [32] by blocking the backdoor path in the SCM (Fig. 2 Right). Specifically, instead of learning the correlation  $P(Y|X)$ , we set our target as  $P(Y|do(X))$ , where  $do(\cdot)$  is the **do-operator** (a.k.a. *do-calculus*), denoting the experimental intervention. Since both  $D$  and  $X$  are accessible in our tasks, we can solve  $P(Y|do(X))$  by applying the backdoor adjustment theorem [32]:

$$P(Y|do(X)) = \sum_d P(Y|X, D = d)P(D = d). \quad (2)$$

Intuitively, the backdoor adjustment removes the risk of spurious correlation arising from  $P(D|X)$  via a two-step strategy. It starts by estimating the causal effect in each stratum of the confounder, followed by summing the effects of all strata, weighted by their known prevalence in the population. By doing so, it ensures that the contribution of the causal effect of an *unobserved* stratum is no different from that of an *observed* one. In this way, the overall causal effect would not be biased towards the observed strata. For example, with the help of the backdoor adjustment, each stratum of the confounder, including *noise*, *blur* and *normal*, will contribute equally to *anger*, forcing the model to learn to recognize *anger* from the intended affective features.

#### 3.3 IERN

To overcome dataset bias in visual emotion recognition, we propose our Interventional Emotion Recognition Network (IERN) by embedding the backdoor adjustment. Compared with heuristic debiasing methods like building larger datasets [29], IERN is designed based on well-studied deconfounding theory. Also, unlike NWGM approximation-based backdoor adjustment models [12, 51] that absorb the probability sum into the network, IERN applies the real intervention  $P(Y|do(X))$ . Fig. 3 gives an overview of the IERN, which is composed of four parts: Backbone, Feature Disentanglement, Confounder Builder and Classifier. The backbone refers to an existing image feature extractor, e.g., VGG [38] or ResNet [15], the

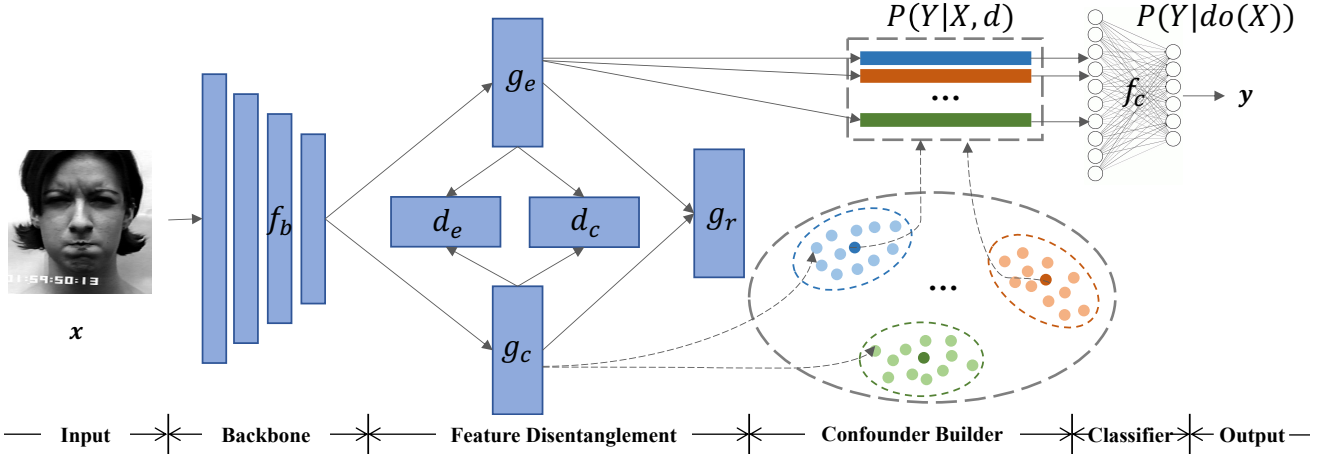


**Figure 3: Overview of Interventional Emotion Recognition Network (IERN).**  $f_b, g_e, d_e, g_c, d_c, g_r$  and  $f_c$  refer to backbone, emotion generator, emotion discriminator, context generator, context discriminator, reconstruction network and classifier, respectively. In training, Feature Disentanglement splits features into emotion and context features. Confounder Builder groups context features and gets their centers as confounder features. Each emotion feature is combined with all strata of the confounder individually, and forwarded to the Classifier. Only the top branch will be leveraged in testing, using the learned confounders.

disentanglement part separates emotion and context features, the confounder builder does the causal intervention, and the classifier predicts the emotion label. Formally,  $f_b, g_e, d_e, g_c, d_c, g_r$  and  $f_c$  refer to backbone, emotion generator, emotion discriminator, context generator, context discriminator, reconstruction network and classifier, respectively.

*Feature Disentanglement.* As mentioned in Section 3.1, without proper handling, context features are mixed with emotion features. Thus, IERN starts by applying feature disentanglement to separate emotion and context features. Specifically, to obtain the clean emotion feature, the disentanglement is conducted by a dual-discriminator structure, consisting of an emotion discriminator  $d_e$  and a context discriminator  $d_c$ , where  $d_e$  is to ensure the extracted feature contains emotional information while  $d_c$  is to ensure that the extracted feature does not contain any context information.

This procedure is implemented by alternating the optimization between the feature generators and the discriminators with the following training objective:

$$\mathcal{L}_e = \min_{d_e^\theta} l_{\text{CE}}(d_e(g_e(f_b(x))), y_e) + \min_{g_e^\theta} l_{\text{MSE}}(d_c(g_e(f_b(x))), \frac{1}{N_c}), \quad (3)$$

where  $l_{\text{CE}}$  and  $l_{\text{MSE}}$  denote the cross-entropy loss and the mean squared error loss, respectively;  $d_e^\theta$  and  $g_e^\theta$  are the trainable parameters of  $d_e$  and  $g_e$ , respectively; and  $g_e(f_b(x))$  is the intended clean emotion feature, obtained by feeding the input image  $x$  first into the backbone  $f_b$  and then into the emotion feature generator  $g_e$ . Also,  $y_e$  is the ground-truth emotion label for  $x$ , and  $N_c$  is the number of levels in the confounder. Intuitively, in Eq. (3),  $d_e$  is optimized to predict the ground truth emotion label given the generated emotion feature  $g_e(f_b(x))$  as input, so as to ensure that  $g_e(f_b(x))$  contains the correct emotion information. Here,  $g_e$  is optimized to

encourage the softmax output of  $d_c$  be equally distributed among all confounder levels, so as to ensure that  $g_e(f_b(x))$  contains no context information.

To obtain clean context features, we adopt a similar optimization approach with the following objective function:

$$\mathcal{L}_c = \min_{d_c^\theta} l_{\text{CE}}(d_c(g_c(f_b(x))), y_c) + \min_{g_c^\theta} l_{\text{MSE}}(d_e(g_c(f_b(x))), \frac{1}{N_e}), \quad (4)$$

where  $d_c^\theta$  and  $g_c^\theta$  are the trainable parameters of the context discriminator  $d_c$  and the context generator  $g_c$ , respectively;  $y_c$  is the confounder label, and  $N_e$  is the number of emotion classes.

To ensure that the separated features fall within reasonable domains, IERN should be capable of reconstructing the base feature  $f_b(x)$ , given the emotion features and the context features as input. Thus, a feature reconstruction loss function is added as

$$\mathcal{L}_r = \min_{g_r^\theta, g_e^\theta, g_c^\theta} l_{\text{MSE}}(g_r(g_e(f_b(x)), g_c(f_b(x))), f_b(x)), \quad (5)$$

where  $g_r^\theta$  is the trainable parameters of the feature reconstruction network  $g_r$ .

*Confounder Builder.* The purpose of the confounder builder is to combine each emotion feature with different context features so as to avoid the bias towards the observed context strata. To limit the diversity of the context features, we propose to use the center of all context features within each specific stratum as a confounder feature. This is reasonable since context features are usually similar within the same stratum while different across different strata. Essentially, a confounder feature represents the *general concept* of a specific stratum. So we adopt the center loss [46] to learn confounder features with the objective function as

$$\mathcal{L}_{\text{CB}} = \min_{C, g_c^\theta} l_{\text{MSE}}(g_c(f_b(x)), C_{y_c}), \quad (6)$$

where  $C_{y_c}$  denotes the learned confounder feature of the  $y_c$ -th stratum of the confounder, and  $C = \{C_1, C_2, \dots, C_{N_c}\}$ , with all being learnable parameters.

*Classifier.* As mentioned in Section 3.2, the backdoor adjustment aims to weigh the causal effect of each stratum with its prevalence in the population, *i.e.*,  $P(D = d)$ , instead of  $P(D = d|X)$ . To ensure fairness, our deconfounded classifier is set such that for any emotion feature, it is present in all confounder strata equally, *i.e.*,  $P(D = d) = 1/N_c$ , via the following training objective:

$$\mathcal{L}_{\text{Cls}} = \min_{f_c^\theta, g_e^\theta, f_b^\theta} l_{\text{CE}}\left(\frac{1}{N_c} \sum_{i=1}^{N_c} f_c(g_r(g_e(f_b(x)), C_i)), y_e\right), \quad (7)$$

where  $f_c^\theta$  denotes the trainable parameters of the classification network  $f_c$ . Given a separated emotion feature  $g_e(f_b(x))$ , IERN reuses the reconstruction network  $g_r$  to combine it with each learned confounder feature  $C_i$ , so as to ensure that for any emotion, the classifier can be challenged with that emotion existing in every stratum of the confounder equally, thus avoiding bias. In other words,  $P(Y|X, D = d)$  is obtained by  $f_c(g_r(g_e(f_b(x)), C_i))$ , while by forwarding  $N_c$  times and taking the average, we have  $P(Y|do(X))$ , where  $P(D = d) = 1/N_c$ .

*Training Phase.* In general, IERN is trained with the weighted combination of the above loss functions. The overall objective is

$$\mathcal{L}_{do} = \lambda_1(\mathcal{L}_e + \mathcal{L}_c + \mathcal{L}_r) + \lambda_2\mathcal{L}_{\text{CB}} + \lambda_3\mathcal{L}_{\text{Cls}}, \quad (8)$$

where  $\lambda_1$ ,  $\lambda_2$  and  $\lambda_3$  are hyper-parameters. IERN is end-to-end trainable, and different components need to be updated sequentially within one training iteration. The detailed training procedure is given in Algorithm 1 (see Section A.2 for technical details).

---

#### Algorithm 1 IERN Training Procedure

---

- 1: **for** number of training iterations **do**
  - 2:   Forward  $f_b, g_e, d_e, g_c, d_c, g_r$
  - 3:   Freeze  $g_e^\theta$  and  $g_c^\theta$ , backward  $d_e$  using 1st term of  $\mathcal{L}_e$  and  $d_c$  using 1st term of  $\mathcal{L}_c$
  - 4:   Freeze  $d_e^\theta$  and  $d_c^\theta$ , backward  $g_e$  using 2nd term of  $\mathcal{L}_e$  and  $\mathcal{L}_r$ ; backward  $g_c$  using 2nd term of  $\mathcal{L}_c$ ,  $\mathcal{L}_r$  and  $\mathcal{L}_{\text{CB}}$ ; backward  $g_r$  using  $\mathcal{L}_r$ ; backward  $C$  using  $\mathcal{L}_{\text{CB}}$
  - 5:   **for**  $i = 1 \rightarrow N_c$  **do**
  - 6:     Forward  $f_c(g_r(g_e(f_b(x)), C_i))$
  - 7:   Backward  $f_c, g_e$  and  $f_b$  using  $\mathcal{L}_{\text{Cls}}$
- 

*Testing Phase.* Given a test image, IERN will predict its emotion by going through only the top branch (see Fig. 3), which is

$$\hat{y}_e = \arg \max \sigma\left(\frac{1}{N_c} \sum_{i=1}^{N_c} f_c(g_r(g_e(f_b(x)), C_i))\right), \quad (9)$$

where  $\sigma$  denotes the softmax function, and  $C_i$  is the confounder feature learned in the training phase. Following the backdoor adjustment theorem, to ensure the prediction of emotion is not biased towards specific strata at test time, we need to combine the emotion feature with each confounder stratum feature and take an average.

**Table 1: Three-fold cross-validation setting. For each fold, image sets denoted with the corresponding number are selected as the test set, with the others as the training set**

	AN	DI	FE	HA	SA	SU
CK+	1	2	3	1	2	3
MMI	3	1	2	3	1	2
Oulu-CASIA	2	3	1	2	3	1

## 4 EXPERIMENTS

We conducted experiments on both facial expression recognition (FER) (Section 4.1) and image emotion recognition (IER) (Section 4.2). For the former, we designed a challenging yet practical out-of-distribution (o.o.d.) test configuration through mixing different benchmarks, *motivated by the fact that in the real world, images provided to practical recognition systems are taken by different people with different preferences, cameras and geographical locations*, and this distribution cannot be controlled [37]. And we conduct ablation study and compare to related SOTA, including DAFL [13] and NWGM-based methods [12], using the introduced configurations. As for the latter, IERN is compared, under the challenging cross-dataset setting, to Curriculum Learning [29], which is the SOTA for unbiased image emotion recognition.

*Implementation details.* To maintain a fair comparison, ResNet-50 [15] was chosen as the backbone  $f_b$  following the setting of [29]. While  $g_e, g_c$  and  $g_r$  are constructed by using the residual block [15] as building blocks,  $d_e$  and  $d_c$  are composed of convolution layers, and  $f_c$  is composed of fully connected layers (see Section A.1 for more details). Note that other backbones or building blocks can also be adopted, as long as they follow the framework depicted in Fig. 3. The hyper-parameters  $\lambda_1$  and  $\lambda_3$  in Eq. (8) were set as default to  $\lambda_1 = \lambda_3 = 1$ , while  $\lambda_2 = 5 \times 10^{-4}$  were set mainly to balance the loss value magnitudes (see Section B for more details). We initialized  $f_b$  with ImageNet [11] pretrained weights, while other components were randomly initialized. An Adam optimizer was used with a learning rate of  $2 \times 10^{-4}$ , decayed using the standard warm-up strategy. All models were trained till converged before testing. Specifically, in the mix-dataset experiments (Section 4.1), IERN were trained for 80 epochs, while in the cross-dataset experiments (Section 4.2), IERN were trained for 140 epochs. All test sets remain untouched during training. We implemented IERN with PyTorch [31].

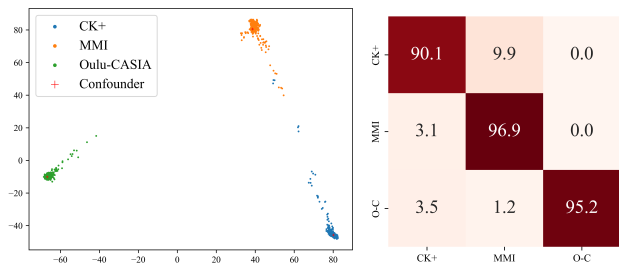
### 4.1 Mix-Dataset Experiments for FER

*Dataset settings.* The facial expression experiments were conducted on three lab-controlled benchmarks, including CK+ [26], MMI [42], and Oulu-CASIA [57]. In all the datasets, we only selected those sequences that contain frontal faces and are labeled with six basic expression labels, *i.e.*, *anger, disgust, fear, happiness, sadness* and *surprise*, resulting in CK+ with 327 sequences of 118 subjects, MMI with 208 sequences of 32 subjects, and Oulu-CASIA with 480 sequences of 80 objects. As a general approach [21], three peak frames were extracted from each sequence for further experiments.

To ascertain the effectiveness of IERN in dealing with dataset bias, practical o.o.d. tests were designed by mixing the three datasets in a three-fold cross-validation setting. With reference to Tab. 1: in

**Table 2: FER accuracy for the comparisons using the *designed o.o.d. setting*. The best results are highlighted in bold**

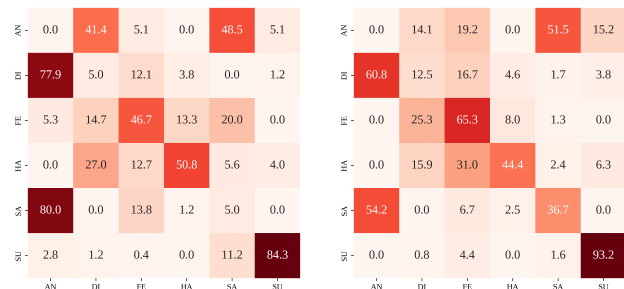
	Anger	Disgust	Fear	Happiness	Sadness	Surprise	Average
Baseline	<b>10.13</b>	30.60	15.29	49.56	10.00	77.12	35.57
Disentanglement	1.27	27.68	18.80	67.19	15.95	80.07	38.95
DACL [13]	5.27	<b>30.68</b>	<b>29.82</b>	47.99	11.90	<b>83.50</b>	38.01
IERN (Ours)	<b>10.13</b>	28.07	23.56	<b>81.85</b>	<b>29.05</b>	79.09	<b>45.50</b>

**Figure 4: Left: t-SNE maps of context and confounder features (best viewed in high-resolution color). Right: confusion matrix of the confounder prediction.**

the first fold, image sets denoted ‘1’, e.g., all *anger* images from CK+, were included in the test set, while the other images were used to construct the training set. Likewise, the second fold comprises a test set of the ‘2’ image sets, and so on. Here we chose to apply a sequence-independent setting rather than a person-independent one, the reason is that using the latter will make the data very unbalanced across different folds, since the numbers of emotions vary across different people on CK+ and MMI. The performance was measured in terms of classification accuracy, averaged across all three folds (% is omitted in all result tables). We point out that under such a setting, the dataset label is the confounder label, i.e.,  $y_c \in \{\text{CK+}, \text{MMI}, \text{Oulu-CASIA}\}$ . Note that we did not specify which parts of the dataset features were biased, but treated all features that can identify each specific dataset jointly as the confounder. This is reasonable since dataset bias in practice can be very complex and it is often hard to identify different bias factors.

*Ablation study of IERN.* We compared IERN to two variants: 1) Baseline, which is the backbone of IERN, i.e., ResNet-50. 2) Disentanglement, which directly feeds the output of  $g_e$  into  $f_c$ , bypassing the Confounder Builder. The results are shown in Tab. 2.

Compared to Baseline, Disentanglement saw a 3.38% improvement in terms of average accuracy. This is because Disentanglement can distill the expected emotion feature whilst dispelling the undesirable confounding feature, so that the classifier can be better learned. This finding has also been explored and verified recently by an existing approach that dealt with biased facial attribute classification [2]. IERN improved on Disentanglement by 6.55%. From a causality point of view, IERN invokes causal intervention, so that it can address the bias better as previously discussed. From a deep learning point of view, IERN can be seen as applying *feature-level data augmentation*. It combines emotion features with all kinds of confounder features to provide coverage even for combinations

**Figure 5: Confusion matrices of accuracy for both Baseline (left) and IERN (right) on the third fold setting.**

missing from training data. So it encounters greater data diversity and is thus more robust than pure disentanglement.

We also evaluated the related SOTA, DACL [13], on the designed setting by training and testing with the released codes. As shown in Tab. 2, IERN outperformed DACL with a healthy margin. Besides, the performance of DACL is close to Disentanglement, since they share similar underlying principles as mentioned in Section 2.

*Confounder features are correctly modeled.* We plotted the extracted context features  $g_c(f_b(x))$  and confounder center features  $C$  using t-SNE. As seen in the left part of Fig. 4, context features were grouped and separated, while confounder features were found near the center of each context feature distribution as expected. Therefore, by using the Confounder Builder, the feature of each stratum of the confounder is correctly modeled, allowing the following *do* intervention to be applied correctly.

*Dataset is the confounder.* The right part of Fig. 4 depicts the accuracy confusion matrix for  $d_c$ , given the extracted context feature  $g_c(f_b(x))$  as input. We can see that the network achieved over 90% accuracy in predicting the confounder / dataset label, which is consistent with the finding of the *Name That Dataset Game* conducted in both [41] and [29]. Compared with the emotion prediction results shown in Tab. 2, it is clear that the network is better at learning to recognize the cognitive level features (dataset characteristics) than to recognize the affective level features (image emotion). Without intervention, the network would thus be biased by the more easily learned dataset features.

*IERN vs Baseline in detail.* To get a closer view of how IERN outperforms Baseline in dealing with dataset bias, the accuracy confusion matrices of both models on the third fold setting are shown in Fig. 5. Compared to IERN, the results of Baseline were biased by the training data. For example, *fear* images in the test

**Table 3: Facial expression recognition accuracy for the comparison with other methods using the *modified setting* (moving 10% of images from the original test set into the training set). The best results for each category are highlighted in bold**

	Anger	Disgust	Fear	Happiness	Sadness	Surprise	Average
Baseline	24.48	46.10	49.44	80.04	46.83	89.31	58.55
Re-sampling	23.78	48.49	57.78	<b>89.73</b>	43.92	90.22	61.59
NWGM-based [12]	30.77	<b>59.74</b>	52.78	81.59	45.24	<b>95.29</b>	63.63
IERN (Ours)	<b>59.44</b>	59.52	<b>60.56</b>	83.92	<b>62.43</b>	93.66	<b>71.71</b>

**Figure 6: Two samples of *anger* from each dataset. See the mouth region, while it is consistently opened within MMI, such manifestation is inconsistent in other two datasets.**

set are from CK+ (see Tab. 1 number 3), Baseline predicted over 50% images as *anger*, *disgust*, *happiness* or *sadness*, which are all related to CK+ in the training set, while IERN alleviated the bias and improved the performance by near 20%.

*Limitation of using dataset as the confounder.* We noticed that the accuracy results of *anger* for both Baseline and IERN are 0 as shown in Fig. 5. The reason is that the manifestation of *anger* in MMI is inconsistent with that in CK+ and Oulu-CASIA, as depicted in Fig. 6, where the mouth region in MMI (consistently opened within MMI) has a very different shape compared to the other two datasets. Since in the third fold, IERN was trained with *anger* images from only CK+ and Oulu-CASIA, it failed to recognize *anger* images in MMI. IERN was rather intended to solve biases caused by dataset characteristics *that are consistently shared across the whole dataset*, e.g., images in MMI have a blue background, CK+ contains mainly gray images, images in Oulu-CASIA are blurry.

The manifestation differences also make the Disentanglement perform much worse than Baseline and IERN in the *anger* expression as shown in Tab. 2. On the first and second folds, *anger* faces in the training set are mixed with images from MMI and another dataset. Under such settings, Feature Disentanglement failed to disentangle emotion and context features due to the inconsistent manifestation, resulting in wrong emotion features. Unlike Disentanglement that predicted emotion labels purely based on the extracted emotion features, our IERN still combined emotion with context features in the following steps before applying classification, allowing it to overcome the flaws to some extent.

*Re-sampling is essentially intervention.* The most widely adopted method in handling dataset bias is to balance the training data through re-sampling. However, in our o.o.d. test setting, the training data does not contain *any* image that shares the same attribute as those in the test set, which makes it *impossible* to directly use re-sampling.

In fact, re-sampling can be considered as a vanilla form of intervention, since it also aims to solve the bias through balancing

the data across all strata of the confounder. For better comparison between IERN and re-sampling, we next *modified the setting* by moving 10% of images (sequence-independent) from the test set into the training set for each attribute in each fold, so that re-sampling can be applied. The performances are reported in Tab. 3.

Compared to Baseline, re-sampling achieved a higher performance with 3.04% improvement. The reason is that re-sampling is approximately intervention, so it can help alleviate the bias and improve the robustness of the model. However, IERN significantly outperformed re-sampling by 10.12%. This is because by modeling unobserved data using confounder features, IERN can improve not only the balance but also the diversity of training data, while re-sampling does not introduce new data.

*Comparison to NWGM-based method.* We also compared IERN to the NWGM-based method [12], given that both methods are based on backdoor adjustment. The confounder features in NWGM are built as a predefined dictionary, by grouping images in the training set according to confounder labels and averaging the extracted features of each group [12, 51].

Using the same *modified setting* as the re-sampling experiment, the results of the NWGM method are shown in Tab. 3. Although both re-sampling and NWGM are approximate interventions, NWGM outperformed re-sampling by 2.04%, suggesting that it is better to model confounders explicitly in the network. Besides, IERN outperformed NWGM by 8.08%. This is because IERN conducts real intervention by modeling confounder features as trainable parameters, while the pre-computed confounders in NWGM might not be sufficiently representative (see Section C for more details).

## 4.2 Cross-Dataset Experiments for IER

*Dataset settings.* Experiments related to image emotion were conducted on three in-the-wild benchmarks, including Deep Sentiment [52], Emotion-6 [29] and WEBEmo [29]. All datasets are based on images collected from the internet, e.g., Flickr, Google. Deep Sentiment contains 1269 images and Emotion-6 has 8350 images, both of which were manually labeled by several human subjects. WEBEmo has around 268,000 images, which were automatically labelled by query keywords. Following [29], we report results based on the binary emotion labels, i.e., *positive* and *negative*.

We followed the same configurations as [29], which mainly used 80% of images for training and the rest for testing. According to the analysis given in [29], the *image scene* is the cause of the bias, and is thus the confounder. Places365-CNNs [59] was used to detect scene categories, which contains over 300 classes. To improve error tolerance and reduce computation, we further developed a *two-step*

**Table 4: Cross-dataset validation for image emotion recognition. Values in cells are the results of Curriculum Learning [29], and values inside brackets are the improvements of IERN. “Self Test” means the self-validation (data from the same distribution) experiments, and “Mean Others” means the average of cross-datasets (data from different distributions) validations**

Train on: \ Test on:	Deep Sentiment	Emotion-6	WEBEmo	Self Test	Mean Others
Deep Sentiment	78.74 [+ 3.01]	49.76 [+ 8.18]	47.79 [+ 3.41]	78.74 [+ 3.01]	48.78 [+ 5.79]
Emotion-6	54.33 [+ 5.19]	77.72 [+ 1.85]	64.30 [+ 0.99]	77.72 [+ 1.85]	59.32 [+ 3.09]
WEBEmo	68.50 [+ 2.13]	78.38 [+ 0.53]	81.41 [+ 0.31]	81.41 [+ 0.31]	73.44 [+ 1.33]

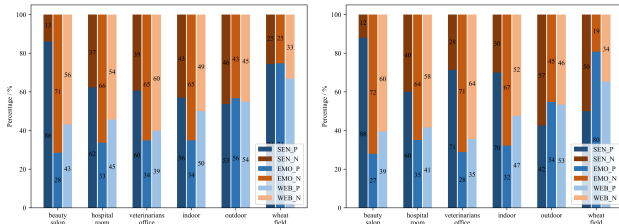


**Figure 7: Emotion distribution within each scene stratum for both training (left) and test sets (right). SEN, EMO and WEB are Deep Sentiment, Emotion-6 and WEBEmo dataset, respectively. P denotes Positive emotion and N denotes Negative emotion (best viewed in high-resolution color).**

*approach* to build confounder labels based on the predicted scene labels. Specifically, scene classes were first grouped into around 30 clusters using k-means, based on their semantic vectors given by GloVe [34]. Secondly, within each dataset, the clusters were sorted by their importance, which is defined as the product of the class prior and the conditional entropy of emotion, i.e.,  $I(c) = P(c) \cdot \sum_{e \in \{p,n\}} P(e|c) \log P(e|c)$ , where  $c$  refers to the cluster label, and  $e$  denotes the binary emotion label, with  $p$  being *positive* and  $n$  being *negative*. The underlying assumption is that if a cluster has more images and more biases, it should be considered more important. The 8 most important clusters were selected as the confounder strata, while other clusters were grouped into *indoor* or *outdoor*, resulting in 10 strata of the confounder for each dataset.

*Comparison with state-of-the-art on cross-datasets.* In order to showcase how dataset bias is alleviated, [29] designed a cross-datasets validation setting. Following their setting, we also trained IERN on the training set of one dataset to convergence, and directly tested it on test sets of all three datasets. Tab. 4 shows the results on all datasets, where the numbers in the cells are the accuracy results of the Curriculum Learning method [29], while the numbers inside the brackets are the improvements achieved by IERN.

Compared with Curriculum Learning, IERN saw improvements in all settings. The reason is this: while Curriculum Learning aims to solve dataset bias through multi-stage fine tuning, IERN explicitly identifies and models the confounders that caused the bias. This allows intervention to be directly applied to balance emotion data across the confounders, which leads to better performance.

We noticed that IERN had a lower improvement when trained on WEBEmo compared to training on the other two datasets, which is

mainly because WEBEmo is already well-balanced. WEBEmo was proposed in [29] as a solution to address the bias problem, with emotion data fairly distributed across scenes. To verify, we plot the emotion distribution within each scene stratum for both training and test sets of all datasets. As shown in Fig. 7, compared with Deep Sentiment and Emotion-6, WEBEmo has better-balanced emotion distributions in many scenes.

We also found that IERN gained less improvement on the self-validation experiments than on cross-dataset ones, especially on Deep Sentiment and Emotion-6. The reason is that self-validation (data from the same distribution) might not be affected by bias [37]. As shown in Fig. 7, within the same dataset, the training and test set have similar bias in the distribution. Thus, although Curriculum Learning might learn biased features during training, it may still achieve good performance on a test set that has the same biases.

Conversely, in the cases of cross-datasets (data from different distributions) validation, this is no longer true. In particular for many scenes, the biases in Deep Sentiment and Emotion-6 are in opposite directions, e.g., in *beauty\_salon*, the emotion of the former tends to be *positive*, while for the latter it tends to be *negative*. So without proper handling, Curriculum Learning may suffer from opposing biases when trained on one dataset and tested on another, while IERN can remove the bias in training via re-balancing, thus achieving higher performance.

## 5 CONCLUSION

We have studied the dataset bias problem in visual emotion recognition from a causality perspective. We have proposed a novel end-to-end trainable framework, IERN, to model the backdoor adjustment theorem of causal intervention in order to achieve unbiased emotion recognition. Extensive experiments on two visual emotion recognition tasks have shown the effectiveness of IERN and its individual components. Future works include applying our solution to other vision tasks and considering more complex confounders, e.g., use gender / ethnicity as confounders, automatically learn the number of confounders by embedding clustering algorithms.

## ACKNOWLEDGMENTS

This study is supported under the RIE2020 Industry Alignment Fund – Industry Collaboration Projects (IAF-ICP) Funding Initiative, as well as cash and in-kind contribution from Singapore Telecommunications Limited (Singtel), through Singtel Cognitive and Artificial Intelligence Lab for Enterprises (SCALE@NTU). This research is also partially supported by FIT Start-up Grant.



## REFERENCES

- [1] Xavier Alameda-Pineda, Elisa Ricci, Yan Yan, and Nicu Sebe. 2016. Recognizing emotions from abstract paintings using non-linear matrix completion. In *IEEE Conf. Comput. Vis. Pattern Recog. IEEE*, 5240–5248.
- [2] Mohsan Alvi, Andrew Zisserman, and Christoffer Nellåker. 2018. Turning a blind eye: Explicit removal of biases and variation from deep neural network embeddings. In *Eur. Conf. Comput. Vis.* 0–0.
- [3] Pierre Baldi and Peter Sadowski. 2014. The dropout learning algorithm. *Artificial Intelligence* 210 (2014), 78–122.
- [4] Yoshua Bengio, Tristan Deleu, Nasim Rahaman, Rosemary Ke, Sébastien Lachapelle, Olexa Bilaniuk, Anirudh Goyal, and Christopher Pal. 2020. A Meta-Transfer Objective for Learning to Disentangle Causal Mechanisms. In *Int. Conf. Learn. Represent.* <https://openreview.net/forum?id=ryxWlgBFPS>
- [5] Michel Besserve, Arash Mehrjou, Rémy Sun, and Bernhard Schölkopf. 2020. Counterfactuals uncover the modular structure of deep generative models. In *Int. Conf. Learn. Represent.* <https://openreview.net/forum?id=SJxDDpEKvH>
- [6] Krzysztof Chalupka, Pietro Perona, and Frederick Eberhardt. 2015. Visual causal feature learning. In *Conf. Uncertainty Artificial Intell.* AUAI Press, Arlington, Virginia, USA, 181–190.
- [7] Shikai Chen, Jianfeng Wang, Yuedong Chen, Zhongchao Shi, Xin Geng, and Yong Rui. 2020. Label Distribution Learning on Auxiliary Label Space Graphs for Facial Expression Recognition. In *IEEE Conf. Comput. Vis. Pattern Recog.* Computer Vision Foundation / IEEE, 13984–13993.
- [8] Yuedong Chen, Guoxian Song, Zhiwen Shao, Jianfei Cai, Tat-Jen Cham, and Jianmin Zheng. 2022. GeoConv: Geodesic guided convolution for facial action unit recognition. *Pattern Recognition* 122 (2022), 108355.
- [9] Yuedong Chen, Jianfeng Wang, Shikai Chen, Zhongchao Shi, and Jianfei Cai. 2019. Facial motion prior networks for facial expression recognition. In *IEEE Vis. Comput. Image Process. IEEE*, 1–4.
- [10] Ciprian Adrian Corneanu, Marc Oliu Simón, Jeffrey F Cohn, and Sergio Escalera Guerrero. 2016. Survey on rgb, 3d, thermal, and multimodal approaches for facial expression recognition: History, trends, and affect-related applications. *IEEE Trans. Pattern Anal. Mach. Intell.* 38, 8 (2016), 1548–1568.
- [11] Jia Deng, Wei Dong, Richard Socher, Li-Jia Li, Kai Li, and Li-Fei-Fei. 2009. Imagenet: A large-scale hierarchical image database. In *IEEE Conf. Comput. Vis. Pattern Recog.* IEEE Computer Society, 248–255.
- [12] Zhang Dong, Zhang Hanwang, Tang Jinhui, Hua Xiansheng, and Sun Qianru. 2020. Causal Intervention for Weakly Supervised Semantic Segmentation. In *Adv. Neural Inform. Process. Syst.*
- [13] Amir Hossein Farzaneh and Xiaojuan Qi. 2021. Facial expression recognition in the wild via deep attentive center loss. In *IEEE/CVF Winter Conf. Appl. Comput. Vis.* 2402–2411.
- [14] Robert Geirhos, Jörn-Henrik Jacobsen, Claudio Michaelis, Richard Zemel, Wieland Brendel, Matthias Bethge, and Felix A Wichmann. 2020. Shortcut Learning in Deep Neural Networks. *arXiv preprint arXiv:2004.07780* (2020).
- [15] Kaiming He, Xiangyu Zhang, Shaoqing Ren, and Jian Sun. 2016. Deep residual learning for image recognition. In *IEEE Conf. Comput. Vis. Pattern Recog.* 770–778.
- [16] Xinya Ji, Hang Zhou, Kaisiyuan Wang, Qianyi Wu, Wayne Wu, Feng Xu, and Xun Cao. 2022. EAMM: One-Shot Emotional Talking Face via Audio-Based Emotion-Aware Motion Model. *ACM SIGGRAPH* (2022).
- [17] Xiuyi Jia, Xiang Zheng, Weiwei Li, Changqing Zhang, and Zechao Li. 2019. Facial emotion distribution learning by exploiting low-rank label correlations locally. In *IEEE Conf. Comput. Vis. Pattern Recog.* 9841–9850.
- [18] Brendan Jou, Subhabrata Bhattacharya, and Shih-Fu Chang. 2014. Predicting viewer perceived emotions in animated GIFs. In *ACM Int. Conf. Multimedia.* 213–216.
- [19] Heechul Jung, Sihaeng Lee, Junho Yim, Sunjeong Park, and Junmo Kim. 2015. Joint fine-tuning in deep neural networks for facial expression recognition. In *Int. Conf. Comput. Vis.* 2983–2991.
- [20] Jiyoung Lee, Seungryong Kim, Sunok Kim, Jungin Park, and Kwanghoon Sohn. 2019. Context-aware emotion recognition networks. In *Int. Conf. Comput. Vis.* 10143–10152.
- [21] Shan Li and Weihong Deng. 2020. Deep facial expression recognition: A survey. *IEEE Trans. Affect. Comput.* (2020).
- [22] Yingjian Li, Yingnan Gao, Bingzhi Chen, Zheng Zhang, Lei Zhu, and Guangming Lu. 2021. JDMAN: Joint Discriminative and Mutual Adaptation Networks for Cross-Domain Facial Expression Recognition. In *ACM Int. Conf. Multimedia.* 3312–3320.
- [23] Shisong Lin, Mengchao Bai, Feng Liu, Linlin Shen, and Yicong Zhou. 2020. Orthogonalization-guided feature fusion network for multimodal 2D+ 3D facial expression recognition. *IEEE Trans. Multimedia* 23 (2020), 1581–1591.
- [24] Mengyi Liu, Shaoxin Li, Shiguang Shan, and Xilin Chen. 2013. Au-aware deep networks for facial expression recognition. In *IEEE Int. Conf. Worksh. Auto. Face and Gesture Recog.* IEEE, 1–6.
- [25] David Lopez-Paz, Robert Nishihara, Soumith Chintala, Bernhard Schölkopf, and Léon Bottou. 2017. Discovering causal signals in images. In *IEEE Conf. Comput. Vis. Pattern Recog.* 6979–6987.
- [26] Patrick Lucey, Jeffrey F Cohn, Takeo Kanade, Jason Saragih, Zara Ambadar, and Iain Matthews. 2010. The extended cohn-kanade dataset (ck+): A complete dataset for action unit and emotion-specified expression. In *IEEE Conf. Comput. Vis. Pattern Recog. Worksh.* IEEE, 94–101.
- [27] Sara Magliacane, Thijs van Ommen, Tom Claassen, Stephan Bongers, Philip Versteeg, and Joris M Mooij. 2018. Domain adaptation by using causal inference to predict invariant conditional distributions. In *Adv. Neural Inform. Process. Syst.* 10846–10856.
- [28] Rongyun Mo, Yan Yan, Jing-Hao Xue, Si Chen, and Hanzi Wang. 2021. D<sup>3</sup>Net: Dual-Branch Disturbance Disentangling Network for Facial Expression Recognition. In *ACM Int. Conf. Multimedia.* 779–787.
- [29] Rameswar Panda, Jianming Zhang, Haoxiang Li, Joon-Young Lee, Xin Lu, and Amit K Roy-Chowdhury. 2018. Contemplating visual emotions: Understanding and overcoming dataset bias. In *Eur. Conf. Comput. Vis.* 579–595.
- [30] Giambattista Parascandolo, Niki Kilbertus, Mateo Rojas-Carulla, and Bernhard Schölkopf. 2018. Learning independent causal mechanisms. In *Int. Conf. Mach. Learn.* PMLR, 4036–4044.
- [31] Adam Paszke, Sam Gross, Francisco Massa, Adam Lerer, James Bradbury, Gregory Chanan, Trevor Killeen, Zeming Lin, Natalia Gimelshein, Luca Antiga, et al. 2019. Pytorch: An imperative style, high-performance deep learning library. In *Adv. Neural Inform. Process. Syst.* 8026–8037.
- [32] Judea Pearl et al. 2000. Models, reasoning and inference. *Cambridge, UK: Cambridge University Press* (2000).
- [33] Judea Pearl and Dana Mackenzie. 2018. *The Book of Why: The New Science of Cause and Effect.* Hachette UK.
- [34] Jeffrey Pennington, Richard Socher, and Christopher D Manning. 2014. Glove: Global vectors for word representation. In *Conference on Empirical Methods in Natural Language Processing.* 1532–1543.
- [35] Jonas Peters, Dominik Janzing, and Bernhard Schölkopf. 2017. *Elements of causal inference.* The MIT Press.
- [36] Delian Ruan, Yan Yan, Shenqi Lai, Zhenhua Chai, Chunhua Shen, and Hanzi Wang. 2021. Feature decomposition and reconstruction learning for effective facial expression recognition. In *IEEE Conf. Comput. Vis. Pattern Recog.* 7660–7669.
- [37] Bernhard Schölkopf, Francesco Locatello, Stefan Bauer, Nan Rosemary Ke, Nal Kalchbrenner, Anirudh Goyal, and Yoshua Bengio. 2021. Toward Causal Representation Learning. *arXiv preprint arXiv:2102.11107* (2021).
- [38] Karen Simonyan and Andrew Zisserman. 2015. Very deep convolutional networks for large-scale image recognition. *Int. Conf. Learn. Represent.* (2015).
- [39] Ning Sun, Qi Li, Ruizhi Huan, Jixin Liu, and Guang Han. 2019. Deep spatial-temporal feature fusion for facial expression recognition in static images. *Pattern Recog. Letters* 119 (2019), 49–61.
- [40] Kaihua Tang, Jianqiang Huang, and Hanwang Zhang. 2020. Long-Tailed Classification by Keeping the Good and Removing the Bad Momentum Causal Effect. In *Adv. Neural Inform. Process. Syst.*
- [41] Antonio Torralba and Alexei A Efros. 2011. Unbiased look at dataset bias. In *IEEE Conf. Comput. Vis. Pattern Recog.* IEEE, 1521–1528.
- [42] Michel Valstar and Maja Pantic. 2010. Induced disgust, happiness and surprise: an addition to the mmi facial expression database. In *Intern. Workshop on EMOTION (satellite of LREC): Corpora for Research on Emotion and Affect.* Paris, France., 65.
- [43] Kaisiyuan Wang, Qianyi Wu, Linsen Song, Zhuoqian Yang, Wayne Wu, Chen Qian, Ran He, Yu Qiao, and Chen Change Loy. 2020. Mead: A large-scale audio-visual dataset for emotional talking-face generation. In *Eur. Conf. Comput. Vis.* Springer, 700–717.
- [44] Xiaohui Wang, Jia Jia, Jie Tang, Boya Wu, Lianhong Cai, and Lexing Xie. 2015. Modeling emotion influence in image social networks. *IEEE Trans. Affect. Comput.* 6, 3 (2015), 286–297.
- [45] Zeyu Wang, Klint Qinami, Ioannis Christos Karakozis, Kyle Genova, Prem Nair, Kenji Hata, and Olga Russakovsky. 2020. Towards fairness in visual recognition: Effective strategies for bias mitigation. In *IEEE Conf. Comput. Vis. Pattern Recog.* 8919–8928.
- [46] Yandong Wen, Kaipeng Zhang, Zhifeng Li, and Yu Qiao. 2016. A discriminative feature learning approach for deep face recognition. In *Eur. Conf. Comput. Vis.* Springer, 499–515.
- [47] Boya Wu, Jia Jia, Yang Yang, Peijun Zhao, Jie Tang, and Qi Tian. 2017. Inferring emotional tags from social images with user demographics. *IEEE Trans. Multimedia* 19, 7 (2017), 1670–1684.
- [48] Siyue Xie and Haifeng Hu. 2018. Facial expression recognition using hierarchical features with deep comprehensive multipatches aggregation convolutional neural networks. *IEEE Trans. Multimedia* 21, 1 (2018), 211–220.
- [49] Kelvin Xu, Jimmy Ba, Ryan Kiros, Kyunghyun Cho, Aaron Courville, Ruslan Salakhudinov, Rich Zemel, and Yoshua Bengio. 2015. Show, attend and tell: Neural image caption generation with visual attention. In *Int. Conf. Mach. Learn.* 2048–2057.
- [50] Yan Yan, Ying Huang, Si Chen, Chunhua Shen, and Hanzi Wang. 2019. Joint deep learning of facial expression synthesis and recognition. *IEEE Trans. Multimedia* 22, 11 (2019), 2792–2807.

- [51] Xu Yang, Hanwang Zhang, and Jianfei Cai. 2021. Deconfounded image captioning: A causal retrospect. *IEEE Trans. Pattern Anal. Mach. Intell.* (2021).
- [52] Quanzeng You, Jiebo Luo, Hailin Jin, and Jianchao Yang. 2015. Robust image sentiment analysis using progressively trained and domain transferred deep networks. In *AAAI*. 381–388.
- [53] Quanzeng You, Jiebo Luo, Hailin Jin, and Jianchao Yang. 2016. Building a large scale dataset for image emotion recognition: the fine print and the benchmark. In *AAAI*. 308–314.
- [54] Zhongqi Yue, Hanwang Zhang, Qianru Sun, and Xian-Sheng Hua. 2020. Interventional Few-Shot Learning. In *Adv. Neural Inform. Process. Syst.*
- [55] Kaihao Zhang, Yongzhen Huang, Yong Du, and Liang Wang. 2017. Facial expression recognition based on deep evolutionary spatial-temporal networks. *IEEE Trans. Image Process.* 26, 9 (2017), 4193–4203.
- [56] Tong Zhang, Wenming Zheng, Zhen Cui, Yuan Zong, Jingwei Yan, and Keyu Yan. 2016. A deep neural network-driven feature learning method for multi-view facial expression recognition. *IEEE Trans. Multimedia* 18, 12 (2016), 2528–2536.
- [57] Guoying Zhao, Xiaohua Huang, Matti Taini, Stan Z Li, and Matti Pietikäläinen. 2011. Facial expression recognition from near-infrared videos. *Image and Vision Computing* 29, 9 (2011), 607–619.
- [58] Sicheng Zhao, Yue Gao, Xiaolei Jiang, Hongxun Yao, Tat-Seng Chua, and Xiaoshuai Sun. 2014. Exploring principles-of-art features for image emotion recognition. In *ACM Int. Conf. Multimedia*. 47–56.
- [59] Bolei Zhou, Agata Lapedriza, Aditya Khosla, Aude Oliva, and Antonio Torralba. 2017. Places: A 10 million Image Database for Scene Recognition. *IEEE Trans. Pattern Anal. Mach. Intell.* (2017).

## A TECHNICAL DETAILS OF IERN

### A.1 Network Architecture

Table 5 provides the detailed structure of our implementation of the Interventional Emotion Recognition Network (IERN). Function name from the PyTorch ‘torch.nn’ package is used to denote the layer, e.g., ‘Conv2d’ refers to ‘torch.nn.Conv2d’, the 2D convolution layer. Note that although emotion generator  $g_e$  (emotion discriminator  $d_e$ ) and context generator  $g_c$  (context discriminator  $d_c$ ) have the same structure, they are declared separately, and their trainable parameters are *not* shared.

### A.2 Implementation

To make clear how different components are optimized sequentially, Algorithm 1 is detailed with PyTorch-like pseudo codes, shown as below.

```

1  # ----- DECLARE OPTIMIZERS -----
2  # optimizer for  $d_e$  and  $d_c$ 
3  optimizer_Dis = Adam([emotion_dis.params(), context_dis.params()])
4  # optimizer for  $g_e$ ,  $g_c$ ,  $C$ , and  $g_r$ 
5  optimizer_Feat = Adam([emotion_gen.params(), context_gen.params(),
6                        center_loss.params(), recon_net.params()])
7  # optimizer for  $f_b$ ,  $g_e$ ,  $g_r$  and  $f_c$ ,
8  # set learning rate of  $g_r$  to 0, to stop it from updating.
9  optimizer_Cls = Adam([backbone.params(), emotion_gen.params(),
10                      {recon_net.params(), 'lr':0.},
11                      classifier.params()])
12 # ----- TRAINING ITERATION -----
13 def optimize_parameters():
14     # line 2 of Algorithm 1
15     forward_Feat()
16     # line 3 of Algorithm 1
17     # use 'detach()' to freeze parameters of
18     # generators within backward_Dis()
19     set_requires_grad(emotion_dis, True)
20     set_requires_grad(context_dis, True)
21     optimizer_Dis.zero_grad()
22     backward_Dis()
23     optimizer_Dis.step()
24
25     # line 4 of Algorithm 1
26     # use 'requires_grad=False' to freeze params of discriminators
27     set_requires_grad(emotion_dis, False)
28     set_requires_grad(context_dis, False)
29     optimizer_Feat.zero_grad()
30     backward_Feat()
31     optimizer_Feat.step()
32
33     # line 5-6 of Algorithm 1
34     #  $C$  is updated above; forward  $N_c$  times inside
35     forward_Cls()
36
37     # line 7 of Algorithm 1
38     # according to  $\mathcal{L}_{Cls}$ ,  $g_r$  should not be updated here
39     optimizer_Cls.zero_grad()
40     backward_Cls()
41     optimizer_Cls.step()
42 # ----- END -----

```

## B HYPER-PARAMETERS SEARCHING

In our experiments, we leveraged an off-the-shelf implementation of center loss<sup>1</sup> for  $\mathcal{L}_{CB}$ , and found that the magnitude of  $\mathcal{L}_{CB}$  is much larger than other loss functions. Therefore, we conducted several experiments on IERN to find the suitable  $\lambda_2$  (see Eq. (8)), by setting  $\lambda_1 = \lambda_3 = 1$  and fixing all other training configurations.

<sup>1</sup><https://github.com/KaiyangZhou/pytorch-center-loss>

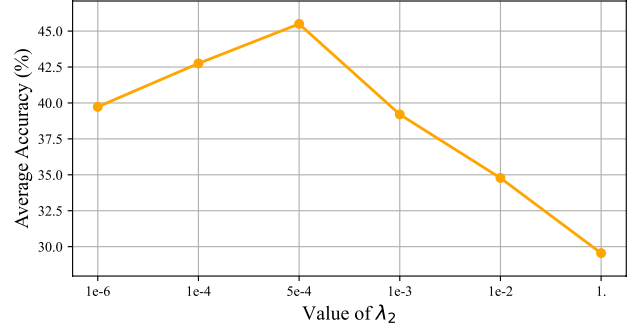


**Figure 8: Hyper-parameters searching on  $\lambda_2$  (Eq. (8) of the main manuscript). We set  $\lambda_2 = 5 \times 10^{-4}$  in our final model.**

As shown in Fig. 8, IERN achieved the best performances when  $\lambda_2 = 5 \times 10^{-4}$ , therefore we used this setting in all following experiments. When  $\lambda_2$  was set to a smaller value, e.g.,  $10^{-6}$ ,  $10^{-4}$ , there is a small drop in the performances. Although confounders were not well learnt in such settings, the final classifier can still be trained sufficiently by  $\mathcal{L}_{Cls}$ , and the performances decrease were mainly caused by the noisy confounders. However, if  $\lambda_2$  was set to a larger value, e.g.,  $10^{-3}$ ,  $10^{-2}$ , 1, performances of IERN decreased dramatically. This is because that IERN failed to optimize Feature Disentanglement and Classifier when  $\mathcal{L}_{CB}$  was way too large, resulting in an unexpected collapse of the full recognition framework.

## C ADVANTAGES OF IERN OVER NWGM

We give a brief introduction of how existing methods [12, 51] use the Normalized Weighted Geometric Mean (NWGM) [49] to approximate the causal intervention. As detailed in Section 3.2, through applying the backdoor adjustment theorem, the model aims to solve

$$P(Y|do(X)) = \sum_d P(Y|X, D = d)P(D = d), \quad (10)$$

where  $X$  and  $D$  are the intended feature and confounder feature, respectively. Here  $P(Y|X, d)$  is normally obtained from the predicted logits of a classification network, i.e.,  $\sigma(f(X, d))$ , where  $\sigma$  denotes the softmax function. Thus, Eq. (10) can be written as

$$P(Y|do(X)) := \mathbb{E}_d[\sigma(f(X, d))]. \quad (11)$$

NWGM is then applied to move the outer expectation into the softmax function, that is

$$\mathbb{E}_d[\sigma(f(X, d))] \stackrel{\text{NWGM}}{\approx} \sigma(\mathbb{E}_d[f(X, d)]). \quad (12)$$

Supposed that the operation of combining  $X$  and  $D$  is linear, then Eq. (12) can be further deduced as

$$\begin{aligned} \mathbb{E}_d[f(X, d)] &= \mathbb{E}_d[W_1x + W_2 \cdot g(d)] \\ &= W_1x + W_2 \cdot \mathbb{E}_d[g(d)], \end{aligned} \quad (13)$$

where  $W_1$  and  $W_2$  both refer to trainable parameters of the fully connected layers. And as a general approach [12, 51],  $\mathbb{E}_d[g(d)]$  is modelled as a attention layer, where the query is set to the base feature and the key is set to a predefined confounder dictionary.

Although existing works have demonstrated the effectiveness of the NWGM-based method, at least three shortcomings can be found.

**Table 5: Detailed structure of all components of IERN. IC: the number of input channels, OC: the number of output channels, K: kernel size, S: stride size, P: padding size, H: height, W: width,  $N_e$ : the number of emotion classes,  $N_c$ : the number of confounder strata. Note that  $g_e$  (or  $d_e$ ) and  $g_c$  (or  $d_c$ ) are declared separately**

Network Component	Detailed Structure
Backbone $f_b$	ResNet-50 (include all but the last average pooling and fully connected layers) Conv2d(IC2048, OC512, K1×1, S1, P0)
Emotion Generator $g_e$ or Context Generator $g_c$	Conv2d(IC512, OC512, K3×3, S1, P1) Residual Block: Conv2d(IC512, OC512, K3×3, S1, P1), BatchNorm2d, ReLU Residual Block: Conv2d(IC512, OC512, K3×3, S1, P1), BatchNorm2d, ReLU
Emotion Discriminator $d_e$ or Context Discriminator $d_c$	Conv2d(IC512, OC512, K4×4, S2, P1), LeakyReLU Conv2d(IC512, OC256, K1×1, S1, P0), LeakyReLU Conv2d(IC256, OC128, K1×1, S1, P0), LeakyReLU Conv2d(IC128, OC64, K1×1, S1, P0), LeakyReLU Conv2d(IC64, OC[ $N_e/N_c$ ], K3×3, S1, P0)
Reconstruction Network $g_r$	Conv2d(IC1024, OC512, K3×3, S1, P1) Residual Block: Conv2d(IC512, OC512, K3×3, S1, P1), BatchNorm2d, ReLU Residual Block: Conv2d(IC512, OC512, K3×3, S1, P1), BatchNorm2d, ReLU Residual Block: Conv2d(IC512, OC512, K3×3, S1, P1), BatchNorm2d, ReLU
Classifier $f_c$	AdaptiveAvgPool2d(H1, W1) Linear(IC512, OC $N_e$ )

Firstly, as pointed out in Section 4.1, the confounder features are not sufficiently representative when constructed via a predefined / pre-computed manner. Secondly, it may not be correct to assume that  $X$  and  $D$  are linearly combined, given that  $D$  could be very complex in practice. Thirdly, NWGM is essentially an approximation and may introduce unintended noise.

By efficiently embedding the backdoor adjustment theorem, our proposed IERN overcomes the aforementioned limitations. Firstly,

IERN directly learns confounder features through disentanglement and leveraging the center loss function. Secondly, IERN reuses the reconstruction network to combine  $X$  and  $D$ , removing the restrictive assumption of the linear combination operation. Thirdly, IERN does not involve NWGM approximation, instead, it forwards the combined features  $N_c$  times to *do the real* intervention. Comparison experiments in Section 4.1 verify the superiority of IERN over NWGM-based methods.